RSC Advances

ROYAL SOCIETY OF CHEMISTRY

www.rsc.org/advances

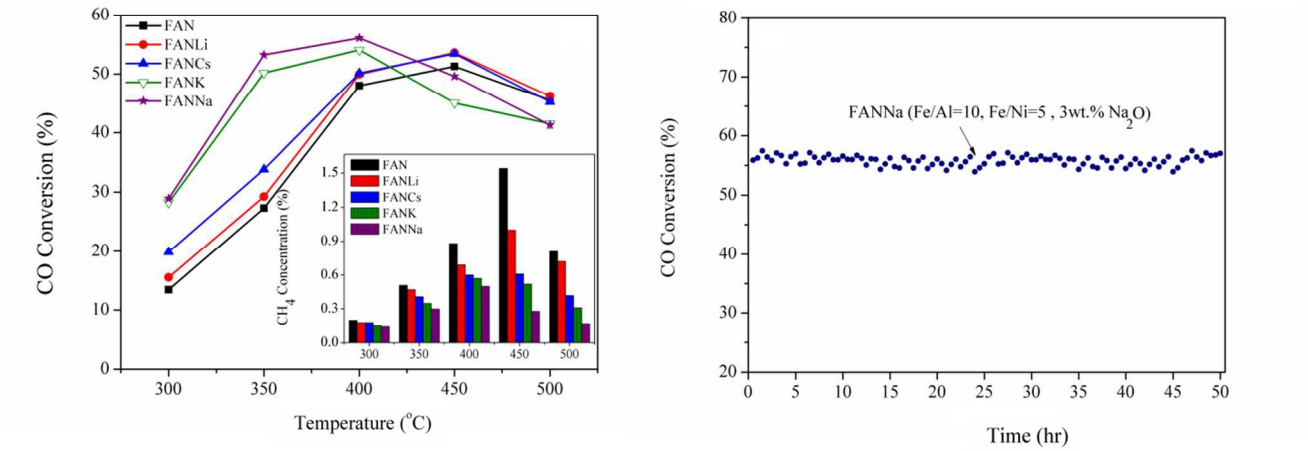

Alkali promoted-Fe-Al-Ni catalysts exhibited higher activity and lower methanation compared to the unpromoted Fe-Al-Ni catalyst in high temperature water gas shift reaction.

RSC Advances

Cite this: DOI: 10.1039/c0xx00000x

www.rsc.org/xxxxxx

PAPER

Preparation of Mesoporous Nanocrystalline Alkali Promoted Chromium Free Catalysts (Fe_2O_3-Al_2O_3-NiO) for High Temperature Water Gas Shift Reaction

Fereshteh Meshkani, Mehran Rezaei*

Received (in XXX, XXX) Xth XXXXXXXXX 20XX, Accepted Xth XXXXXXXXX 20XX
DOI: 10.1039/b000000x

Water gas shift reaction is one of the oldest heterogeneous catalytic reactions operating in industry for H_2 production with high purity and CO removal from syngas. Typical industrial catalyst for high temperature water gas shift (HTS) reaction is Fe-Cr-Cu, but has environmental and safety concerns related to chromium content, which has been regarded as hazardous material. In this study, the effect of addition of alkali metal oxide promoters to chromium free Fe_2O_3-Al_2O_3-NiO catalyst was investigated in HTS reaction. Nanocrystalline promoted chromium free catalysts with mesoporous structure were synthesized by coprecipitation and impregnation methods. Brunner-Emmett-Teller (BET), X-ray diffraction (XRD), temperature-programmed reduction (TPR) and desorption (TPD), scanning and transmission electron microscopies (SEM, TEM) techniques were performed to elucidate the HTS catalytic activity based on the influence of promoters addition on the catalyst structure. The results indicated that the addition of alkali promoters was effective in suppressing methanation as well as in promoting HTS reaction activity for CO removal, which was related to the increment of amount in weakly basic sites through promoter addition. The results revealed that the Fe_2O_3-Al_2O_3-NiO (FAN) catalyst promoted by Na exhibited the highest catalytic activity and the lowest methanation among the investigated catalysts under low steam/gas molar ratio, which favored methane formation. Furthermore, this catalyst presented higher CO removal activity than the commercial chromium containing one. Moreover, the effect of Na content on the structural and catalytic properties of the FANNa catalysts was investigated and the results indicated that the catalyst with 3wt.% Na showed high activity and stability during 50 h time on stream.

Introduction

Recently, a different type of environmental issue is addressed in the area, which is involved with the catalyst materials used for hydrogen production (steam or dry reforming, water gas shift reaction, preferential oxidation, etc.). The issue begins to be raised as the disposal of hazardous and toxic catalyst materials come under the controlling terms of the environmental regulations of various countries in EU and US [1-4]. The water gas shift reaction for CO removal and H_2 production from syngas is a crucial unit reaction in the syngas and/or hydrogen production processes [5-7].

To produce high purity hydrogen at the highest possible CO conversions, two-stage are used: a high temperature shift (HTS) reactor operating at 320–450°C with a catalyst based on iron oxide structurally promoted with chromium oxide (Fe_2O_3-Cr_2O_3), and a low temperature shift (LTS) reactor operating at a temperature range of 200–250°C with Cu-ZnO-Al_2O_3 catalyst [8-10]. The conventional high temperature water gas shift (HTS) catalyst is Fe_2O_3-Cr_2O_3-CuO, in which chromium is a structural promoter, avoiding the sintering of the active phase of catalyst (Fe_3O_4) during the reaction [11]. In addition, commercial catalysts include 2–4 wt. % CuO as a promoter, which may provide additional active sites [12]. The fresh and spent commercial HTS Fe-Cr catalysts usually contain levels of about 1-2 wt.% hexavalent chromium (Cr^{6+}), a very toxic heavy metal to humans, organisms, or cells, and an undesirable environmental contaminant, which is difficult to properly dispose [13]. Especially in Europe, RoHS (Restriction of Hazardous Substances) restricts the use of six hazardous materials including Cr^{6+} in all the electronic/electrical devices and components [14].

Notes and references
*Catalyst and Advanced Materials Research Laboratory, Chemical Engineering Department, Faculty of Engineering, University of Kashan, Kashan, 87317, I.R. Iran. Fax: +98-03155559930; Tel: +98-03155912831
E-mail: Rezaei@kashanu.ac.ir

Many researches about Cr-free catalysts for HTS reaction have been performed in the last two decades [15-18]. Recently, Fe-Al-Cu was known as a highly active catalyst for HTS reaction [16-17]. Although the Fe-Al-Cu catalysts showed high activity but reported results also indicated that at higher Cu levels, deactivation of the catalyst with time-on-stream may be an issue [19]. Furthermore, nickel was selected as the substitution metal for Cr in the Fe-based catalyst due to its wide use as an active species of catalysts for syngas (CO, H_2)-related reactions [20-22] and various CO removal reactions [23-24]. Moreover, the incorporation of Ni into the Fe oxide structure was reported to enhance the thermal stability and catalytic activity compared to the single Fe oxide catalysts [25-26]. But the main drawback is the production of a small amount of CH_4 produced by methanation reaction [24]. However, in a standpoint of WGSR operation, any methanation is in principle undesirable due to the associated hydrogen consumption. Therefore, further researches are required to find a proper promoter for the Fe/Ni-based catalysts, which is capable of enhancing the HTS activity while suppressing methanation [4]. It is known that the addition of alkali and alkaline earth metals can suppress the methanation activity. On the other hand, previous works have also demonstrated that Ni catalyst promoted with potassium exhibited high catalytic performance for the WGS process [27]. The effect of Cs addition to the Fe-Ni catalysts was investigated by Lee et al. [7]. They found that the Cs/Ni/Fe catalysts containing 3.9–6.0 Cs wt.% showed high CO conversion and low methane formation due to increasing the amount in weakly basic sites through Cs promotion. In this paper, the effect of addition of alkali promoters on the CO removal performance and methane formation of chromium free Fe_2O_3-Al_2O_3-NiO catalyst was investigated.

Experimental

Materials

The starting materials were Fe $(NO_3)_3.9H_2O$, Al $(NO_3)_3.9H_2O$, Ni $(NO_3)_2.3H_2O$, Na_2CO_3, KNO_3, $LiNO_3$, $CsNO_3$ and NaOH. All chemicals were of analytical grade and used without further purification. Distilled deionized water was used for the preparation of all aqueous solutions.

Catalyst preparation

The prepared catalysts and their abbreviations are listed in Table 1. The unpromoted catalyst and catalysts promoted by Li and Cs were prepared by coprecipitation method. Depending on the catalyst composition the desired amounts of metal salt precursors were dissolved in distilled water. After that an aqueous solution of NaOH (1 M) was added dropwise at room temperature to the prepared solution containing metal salt precursors under rapid stirring by careful pH adjustment to 10. After precipitation, the slurry was refluxed at 60°C for 5h under continuous stirring. Then the mixture was cooled to room temperature, filtered and washed with hot deionized water for an effective removal of ions. The final product was dried at 90 °C for 24 h and calcined at 400°C for 4 h in air atmosphere with the heating rate of 5 °C/min. For the K and Na promoted FAN catalysts, firstly the FAN catalyst was prepared by coprecipitation method as described above and calcined at 350 ^oC for 4 h. After that the FAN powder was impregnated with aqueous solutions of $K(NO_3)$ and Na_2CO_3 to prepare K and Na promoted FAN catalysts with desired promoter contents. Then the impregnated powders were dried at 80^oC and calcined at 400 ^oC for 4 h in static air atmosphere.

Characterization

The crystalline structure of the prepared catalysts was determined by X-ray powder diffraction (XRD) using a X-ray diffractometer (PANalytical X'Pert-Pro) using a Cu-Kα monochromatized radiation source and a Ni filter. The specific surface area was evaluated by the BET method using N_2 adsorption at –196 °C using an automated gas adsorption analyzer (Tristar 3020, Micromeritics). The Barrett, Joyner and Halenda (BJH) method was used to determine the pore size distribution from the desorption branch of the isotherm. Temperature-programmed reduction (TPR) was carried out using an automatic apparatus (Chemisorb 2750, Micromeritics) equipped with a thermal conductivity detector. Before the TPR experiment, the fresh sample (ca. 50 mg) was treated under an inert atmosphere at 250 °C for 2 h, and then subjected to a reduction treatment with a heating rate of 10 °C/min in a reducing gas flow (20 mL/min) containing a mixture of H_2:Ar (10:90).

Temperature programmed desorption behavior of CO_2 and CO was carried out on the same apparatus as for H_2-TPR. Before the experiment, the catalyst was reduced at 400°C under a reducing gas flow (30 mL/min) containing a mixture of H_2:Ar (10:90) for 2h. After that the reduced catalyst was saturated by the CO or CO_2 at room temperature for 1 h and then the saturated sample was purged with He at room temperature for 30 min. TPD was carried out with a ramp of 10ºC min^{-1} from room temperature to a needed temperature under He stream.

The elemental analysis of various elements was done by using Atomic Absorption Spectrophotometer (AAS) GBC-902. The surface morphology of the catalysts was observed with scanning and transmission electron microscopies techniques (SEM, Vega@Tescan and TEM, Philips CM30).

Catalytic reaction

The high temperature water gas shift reaction tests were performed in a quartz tubular fixed bed flow reactor (i.d. 8 mm) under atmospheric pressure. The thermocouple was inserted in bottom of the catalyst bed to measure the reaction temperature. The total catalyst charged for each reaction was held constant (100 mg and with particle size of 0.25-0.5 mm). A gaseous mixture of 30% CO, 60% H_2, 10% CO_2 and a water steam with H_2O/dry gas molar ratio of 0.3 were supplied to the catalyst bed. The gas and water flow rates were controlled by the mass flow controllers and a programmable syringe pump, respectively.

Prior to reaction, the catalysts were reduced using a gaseous mixture of 30% CO, 60% H_2, 10% CO_2 and a water steam with H_2O/dry ratio of 0.3 at 400 ^oC for 2 h. The activity tests were carried out at different temperatures ranging from 300 ^oC to 500 ^oC in steps of 50 ^oC. Before each analysis, the effluent passed through a water-trap to remove the water from the product stream. The gas composition was analyzed by a HID YL-6100 gas chromatograph equipped with a Carboxen 1010 column.

RSC Advances

Cite this: DOI: 10.1039/c0xx00000x

www.rsc.org/xxxxxx

PAPER

Table 1. Structural properties of the prepared catalysts

Sample Code	Catalyst	Nominal Composition (wt. %)	Elemental composition (wt. %)	Surface area ($m^2 g^{-1}$)	Pore volume ($cm^3 g^{-1}$)	Pore size (nm)	Particle Size (nm)	$Fe_2O_3 \rightarrow Fe_3O_4$ phase transformation (°C)
F	Fe_2O_3	100%	N.M.	14.1	0.1	13.8	81.0	433
FA	Fe/Al=10	88.3 % Fe_2O_3- 11.7 % Al_2O_3	88.0 % Fe_2O_3- 12 % Al_2O_3	152.8	0.3	4.5	7.6	400
FAN	Fe/Al=10, Fe/Ni=5	76.3 % Fe_2O_3- 10.1 % Al_2O_3- 13.6 % NiO	75.7 % Fe_2O_3- 10.5 % Al_2O_3- 13.8 % NiO	177.4	0.3	4.4	6.4	347
FANNa	Fe/Al=10, Fe/Ni=5, 3 wt.% Na_2O	74.0 % Fe_2O_3- 9.8 % Al_2O_3- 13.2 % NiO – 3% Na_2O	73.1 % Fe_2O_3- 10.2 % Al_2O_3- 13.6 % NiO – 3.1% Na_2O	147.7	0.3	4.7	7.8	376
FANLi	Fe/Al=10, Fe/Ni=5, 3 wt.% Li_2O	74.0 % Fe_2O_3- 9.8 % Al_2O_3- 13.2 % NiO – 3% Li_2O	74.5 % Fe_2O_3- 9.3 % Al_2O_3- 13.3 % NiO – 2.9% Li_2O	192.5	0.3	4.3	6.0	341
FANK	Fe/Al=10, Fe/Ni=5, 3 wt.% K_2O	74.0 % Fe_2O_3- 9.8 % Al_2O_3- 13.2 % NiO – 3% K_2O	73.7 % Fe_2O_3- 10.0 % Al_2O_3- 13.1 % NiO – 3.2% K_2O	126.4	0.2	4.6	9.1	370
FANCs	Fe/Al=10, Fe/Ni=5, 3 wt.% Cs_2O	74.0 % Fe_2O_3- 9.8 % Al_2O_3- 13.2 % NiO – 3% Cs_2O	74.1 % Fe_2O_3- 10.1 % Al_2O_3- 12.6 % NiO – 3.2% Cs_2O	182.6	0.3	4.5	6.2	347

Results and discussion

The structural properties of the Fe, Fe-Al, Fe-Al-Ni and promoted Fe-Al-Ni catalysts with alkali metal oxides (Na_2O, K_2O, Li_2O and Cs_2O) are presented in Table 1. Pure iron oxide (F) exhibited a low specific surface area and pore volume. The presence of either Al or two promoters i.e. Al and Ni increased the BET surface area and pore volume of the pure iron oxide. Conversely addition of these promoters decreased the pore size of the prepared catalysts. As reported in our previous work, aluminum is known as a textural promoter and employed as a spacer to protect iron oxide from sintering by keeping the particles apart from each other and increase the specific surface area [28].

Moreover, increasing in the BET surface area of the Fe-Al catalyst by addition of nickel confirms the role of Ni as a structural promoter.

It is seen that for Li and Cs promoted FAN catalysts, both the BET surface area and pore volume increased possibly due to the differences in pore size and pore volume of the prepared catalysts. But catalysts promoted by K and Na possessed lower BET surface area and pore volume compared to the FAN catalyst, which caused by the plugging of the pores with K and Na oxides in impregnation synthesis step. In addition, the theoretical particle sizes (samples were assumed spherical in particles shape) were calculated from the measured specific surface areas according to the following equation:

$$D_{BET} = 6000/(\rho.S) \quad (1)$$

Where D_{BET} is the equivalent particle diameter in nanometers, ρ is the density of the material in g/cm^3 and S is the specific surface area in m^2/g. The results indicated that the Li and Cs promoted FAN catalysts possessed the smaller particle size, while K and Na promoted FAN catalysts showed bigger particle size compared to the unpromoted FAN catalyst.

The pore size distributions of the prepared catalysts are shown in Fig. 1a. The BJH analysis indicates the single modal pore size distribution for the prepared catalysts with major sizes of 2-50 nm. Pure iron oxide showed a broad pore size distribution centered at 22 nm. The pore size distributions of the other catalysts are closely dependent on the type of promoter added to the iron oxide.

Addition of Al and Ni significantly affected the pore size distribution of the pure iron oxide and FA and FAN catalysts exhibited the narrowest pore size distribution centered at 4-5 nm. Moreover, it is seen that addition of alkali promoters to the FAN catalyst slightly shifted the pore size distribution to the smaller sizes.

The N_2 adsorption/desorption isotherms of the prepared samples are shown in Fig. 1b and implying type IV as classified by IUPAC ((International Union of Pure and Applied Chemistry)

[29]. These samples exhibited H2 type hysteresis loop, which is characteristic to the pores with narrow necks and wide bodies. However, this assignment was considered to be oversimplified recently, including in a review by Kruk and Jaroniec [30]. H2 hysteresis loops were attributed to the relatively uniform channel-like pores. Isotherms with type H2 loops tend to level off when the pressure is close to the saturation pressure [31].

In addition, the hysteresis loop of the pure iron oxide was formed at the highest p/p^0 relative pressure, indicating that this sample exhibited a broad pore size distribution, Fig. 1a. For other promoted catalysts the hysteresis loop was observed at lower p/p^0 relative pressures, indicating that these samples have narrower pore size distributions.

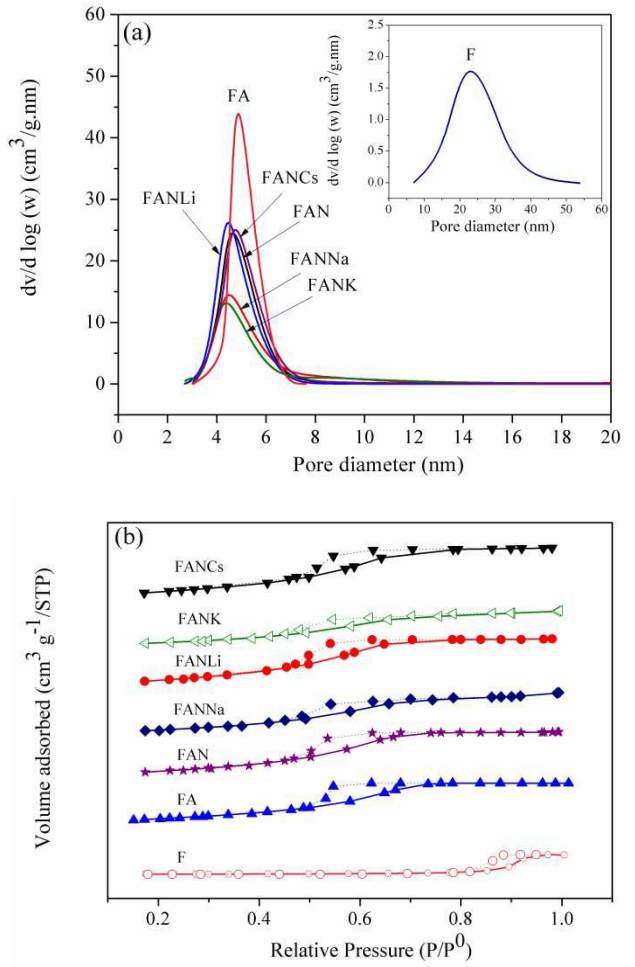

Figure 1. (a) Pore size distributions and (b) N_2 adsorption/desorption isotherms of the prepared catalysts calcined at 400°C

The XRD patterns of the prepared catalysts are presented in Fig. 2a. Pure iron oxide (F) showed a highly crystallized α-Fe_2O_3 phase, while FA catalyst showed the XRD pattern with significantly lower degree of crystallinity than pure iron oxide. The lower peak intensities of Al-doped iron oxide catalyst are attributed to the formation of highly small particles in this sample. The effect of alumina could be regarded as isolator, which prevents the severe sintering of FeO_x phase during the post-treatment processes. As can be seen in FAN catalyst, addition of Ni did not affect the degree of crystallinity and no other phases beside hematite were detected. This may be related to the fact that Ni is expected to entrance into the magnetite lattice rather than to segregate as another phase due to its similar ionic radius to the iron atom [32-33]. For other promoted catalysts no peaks related to promoters were observed due to low content of them in catalyst composition.

TPR analysis was carried out over F, FA, FAN and promoted FAN by alkali metal oxides to provide insight on the reduction behavior of the prepared catalysts and the obtained results are presented in Fig. 2b. Pure iron oxide displayed three man reduction peaks. The first peak at 433 °C was related to the reduction of $Fe_2O_3 \rightarrow Fe_3O_4$. The second reduction peak at 650 °C was attributed to the reduction of $Fe_3O_4 \rightarrow FeO$ and finally the transition of $FeO \rightarrow Fe$ was occurred at temperature higher than 700 °C.

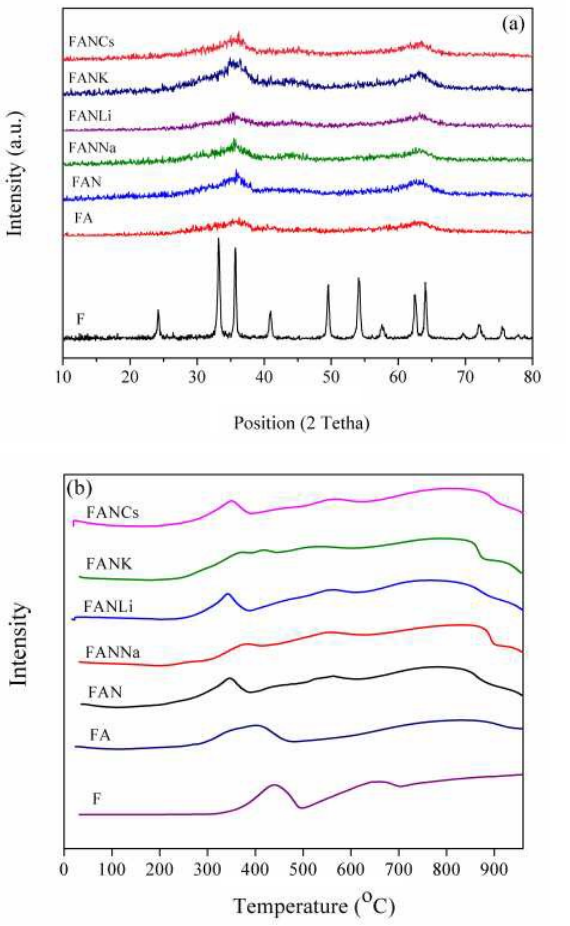

Figure 2. (a) XRD patterns and (b) TPR profiles of the prepared catalysts calcined at 400°C

It is seen that addition of Al to F catalyst (FA) decreased the reduction temperature of hematite to magnetite, Table 1. For this catalyst the reduction of $Fe_3O_4 \rightarrow FeO$ and $FeO \rightarrow Fe$ was observed at temperature higher than 600°C.

RSC Advances

Cite this: DOI: 10.1039/c0xx00000x

www.rsc.org/xxxxxx

PAPER

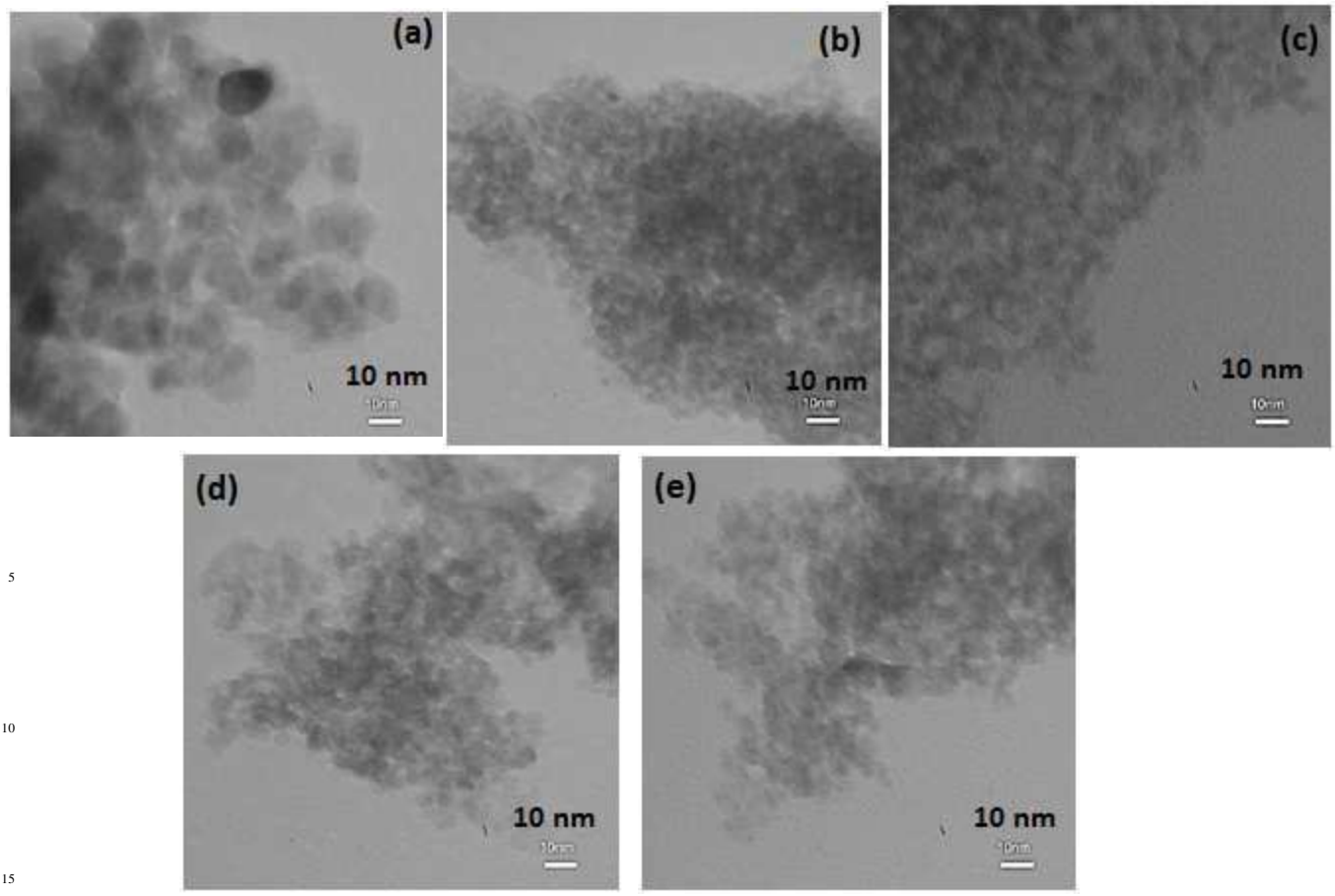

Figure. 3. TEM image of (a) FANK, (b) FAN, (c) FANLi, (d) FANCs and (e) FANNa fresh catalysts

Comparison of the TPR profile of FA and FAN catalysts and the results given in Table 1 indicated that nickel favors the active phase formation by decreasing the needed temperature for reduction of $Fe_2O_3 \rightarrow Fe_3O_4$. In the absence of Ni (FA catalyst), the reduction of hematite to magnetite starts at 400˚C. In addition, the dispersed NiO in the FAN catalyst was reduced at 440°C and another reduction peak observed at 550°C was assigned to the reduction of nickel-containing species including $NiFe_2O_4$. The last reduction peak at temperature higher than 700°C was related to reduction FeO to Fe. TPR profiles of promoted FAN catalysts shown in Fig. 2b confirmed that K and Na promoters make the reduction of $Fe_2O_3 \rightarrow Fe_3O_4$ harder, while addition of Li to FAN catalyst facilitated this transition. Furthermore, addition of Cs did not affect the reduction characteristic of the FAN catalyst, Table 1.

The TEM images of the prepared catalysts with different promoters are shown in Fig 3. It is seen that all the prepared catalysts exhibited nanocrystalline structure with crystallite size smaller than 10 nm, which is in agreement with the particle size determined by the BET area (Table 1). As can be seen, the FANK catalyst showed bigger crystallite size than those observed for other prepared catalysts. This catalyst also exhibited the lowest BET surface area.

CO conversion and the amount of CH_4 concentration over the prepared catalysts at high temperature water gas shift reaction is shown in Fig. 4a. For better comparison the HTS reaction was carried out under low steam/gas molar ratio, which favors the methane formation. As can be seen, methane was produced over all catalysts and its concentration increased by increasing reaction temperature up to 450°C. Further increase in temperature has a negative effect on the methanation due to exothermic nature of this reaction.

The results indicated that the promoted-FAN catalysts exhibited higher CO conversion and lower methane concentration compared to the FAN catalyst indicating the role of alkali metals for improving HTS reaction and suppression of methanation.

RSC Advances

Cite this: DOI: 10.1039/c0xx00000x

www.rsc.org/xxxxxx

PAPER

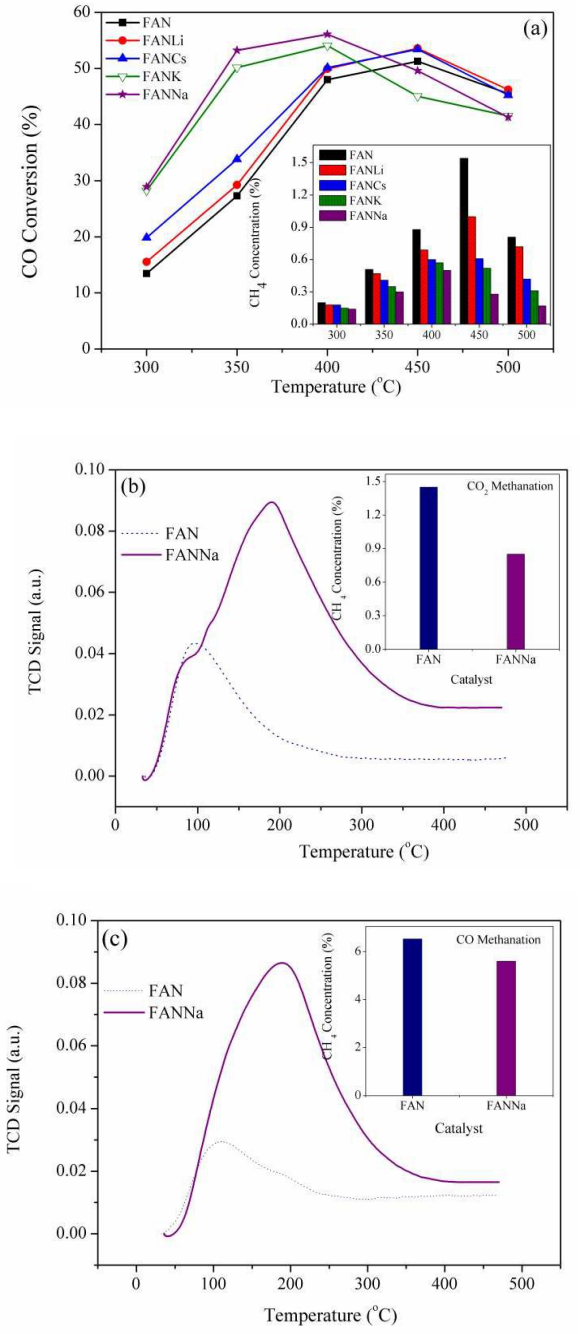

Figure 4. (a) CO conversion of the prepared catalysts calcined at 400 °C, GHSV= 3×10^4mL/h.g_{cat}, and steam/gas=0.3, (b) CO_2-TPD and CO_2 methanation over FAN and FANNa catalysts at 400°C, feed composition: H_2/CO_2=4, GHSV= 3×10^4mL/h.g_{cat} (c) CO-TPD profiles of the FAN3Na catalyst at 400 °C , feed composition: H_2/CO=3, GHSV= 3×10^4mL/h.g_{cat}

In addition, among the investigated catalysts, FANNa catalyst possessed the highest activity and the lowest methanation. The activity results showed that the CO conversion of FANNa is surprisingly higher than unpromoted FAN catalyst.

CO_2-TPD analysis was employed to investigate the effect of Na addition on the adsorption behavior of CO_2 on FAN catalyst. As shown in Fig. 4b, the CO_2-TPD profile of FAN catalyst showed a broad CO_2 desorption peak around 50-300 °C indicating the week basic sites on the surface of the FAN catalyst, which is similar to the result of Gao et al. that claimed that the weakly basic sites (surface hydroxyl groups) of Ni/Fe oxides are characterized by CO_2 desorption peaks around 50-400 °C [34]. The CO_2-TPD of the FANNa catalyst clearly showed that addition of Na to the FAN catalyst significantly promoted the CO_2 adsorption implying more basic sites over the FANNa catalyst.

The CO-TPD results of FNA and FNANa catalysts are presented in Fig. 4c. As can be seen a main broad desorption peak at temperature lower than 300 °C corresponding to the weak CO adsorption was observed for FAN catalyst. The results demonstrated that addition of Na significantly affected the CO adsorption and caused a significant increase in the intensity of CO desorption peak. Many results have been reported according to the improvement of CO adsorption by addition of alkali metals such as potassium [35-38]. Miller and Moskovits [39] reported that as the K level increases, the extent of CO adsorption is significantly increased. Wan et al. [40] investigated the effect of K addition on the adsorption behavior of iron based catalysts and found that potassium donates electrons to iron and facilitates CO chemisorption, since CO tends to accept electrons from iron. Thus the addition of K promoter facilitates the CO adsorption.

The CO_2 and CO methanation test results for the FAN and FAN3Na catalysts at 400°C are shown in Fig.4b and 4c (upper inset), respectively. The results clearly revealed that addition of Na to FAN catalyst suppressed both CO_2 and CO methanation activity of the FAN catalyst. Considering the water gas shift and methanation activity of FAN and FANNa catalysts, it was expected that the increment of such weakly basic sites of the catalyst would effectively enhance the HTS activity (through formation of format intermediate) and the selectivity of WGSR against methanation [41-42].

The structural properties of the FAN catalysts with different Na contents are presented in Table 2. It is seen that addition of Na to FAN catalyst decreased the BET surface area and pore volume and increased the average pore size. The decrease in the BET surface area and pore volume after addition of Na may be caused by a partial blockage of the FAN pores by Na_2O clusters and/or a partial collapse of the mesoporous structure. The results showed that increasing in Na content led to a decrease in BET surface area and pore volume.

Table 2. Structural properties of the catalysts with various Na contents

Sample Code	Composition	Surface area (m^2 g^{-1})	Pore volume (cm^3 g^{-1})	Pore size (nm)	Particle Size (nm)*
FAN1.5Na	Fe/Al=10, Fe/Ni=5, 1.5 wt.% Na_2O	149.7	0.3	4.6	7.6
FAN3Na	Fe/Al=10, Fe/Ni=5, 3 wt.% Na_2O	147.7	0.3	4.7	7.8
FAN6Na	Fe/Al=10, Fe/Ni=5, 6 wt.% Na_2O	109.7	0.2	4.8	10.7
Fe-Cr-Cu Commercial Catalyst	-	76.0	0.2	10.4	15.0
Reduced-FAN3Na	Fe/Al=10, Fe/Ni=5, 3 wt.% Na_2O	38.8	0.2	18.6	29.7
Spent- FAN3Na	Fe/Al=10, Fe/Ni=5, 3 wt.% Na_2O	22.9	0.1	27.1	50.2

*:Determined by BET area

In addition, as can be seen the particle size also increased by increasing in Na content. However, the promoted catalysts exhibited higher surface area and smaller particle size compared to commercial catalyst.

The pore size distributions and N_2 adsorption/desorption isotherms are shown in Fig. 5a and 5b, respectively. It is seen that the promoted catalysts exhibited narrow pore size distributions centered at around 4.5 nm. The results revealed that increasing in Na content did not have a significant effect on the pore size distribution.

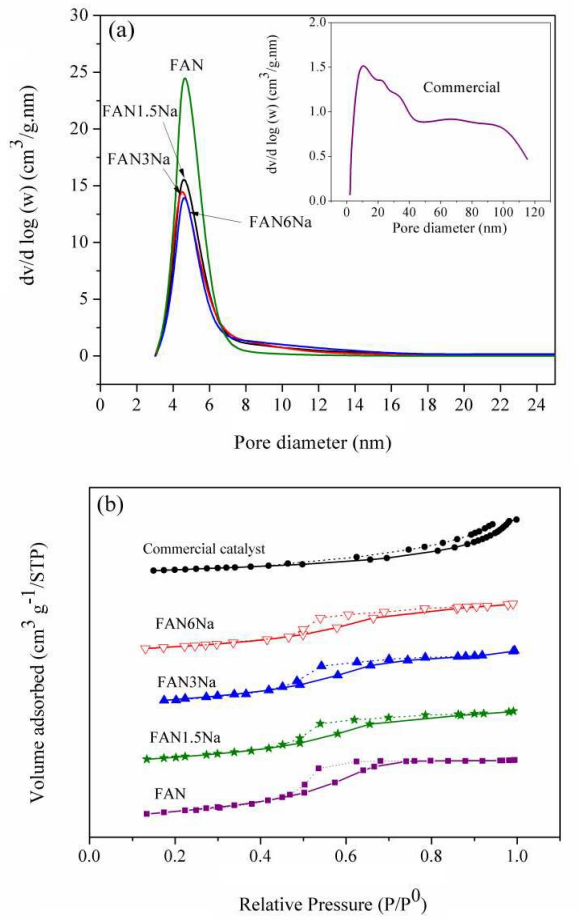

Figure. 5. (a) Pore size distributions and (b) N_2 adsorption/desorption isotherms of the commercial and FANNa catalysts with different Na contents calcined at 400°C

As can be seen, the commercial catalyst exhibited a broad pore size distribution in meso and macro regions. The N_2 adsorption/desorption isotherms of the promoted catalysts showed the existence of IV type isotherm with H2 hysteresis loop. The formation of hysteresis loops at low relative pressures indicates the narrow pore size distribution with small pores as shown in Fig. 5a.

As can be seen the shape of isotherms did not change after addition of Na to the FAN catalyst, indicating the similar pore size distributions for the prepared catalysts. The commercial catalyst exhibited a type V isotherm with H3-type hysteresis loop, which is usually attributed to large mesopores or macropores surrounded by a matrix of much smaller pores. For the commercial catalyst the hysteresis loop was formed at higher p/p0 relative pressure, which shows that this catalyst exhibited a broad pore size distribution, ranging from mesopores to macropores, Fig. 5a (upper inset).

The XRD patterns of the promoted FAN catalysts with different Na contents are shown in Fig. 6a. The XRD results revealed that the promoted samples exhibited a low degree of crystallinity and increasing in Na content did not change the XRD patterns. All promoted catalysts exhibited the similar XRD patterns and no peaks related to Na species were observed. However, the commercial catalyst exhibited higher crystallinity and the sharp peak at around 26° was related to graphite, which used during the shaping process of catalyst powder.

The effect of Na_2O content on the reduction behaviors of the promoted FAN catalysts is shown in Fig. 6b. The obtained results revealed that increasing in Na2O content caused a slight increase in reduction temperature of hematite to magnetite. In addition, the T_{Max} of the reduction peaks observed at 550-600°C (related to reduction of nickel -containing species including $NiFe_2O_4$) was shifted to lower temperatures with increasing in Na2O content.

For the commercial catalyst, two main reduction peaks were observed in TPR profile. The reduction peak at lower temperature (316 °C) was attributed to reduction of CuO to metallic copper and CrO_3 to Cr_2O_3 and reduction of Fe_2O_3 to Fe_3O_4 and the second broad reduction peak was related to reduction of Fe_3O_4 to FeO and metallic iron.

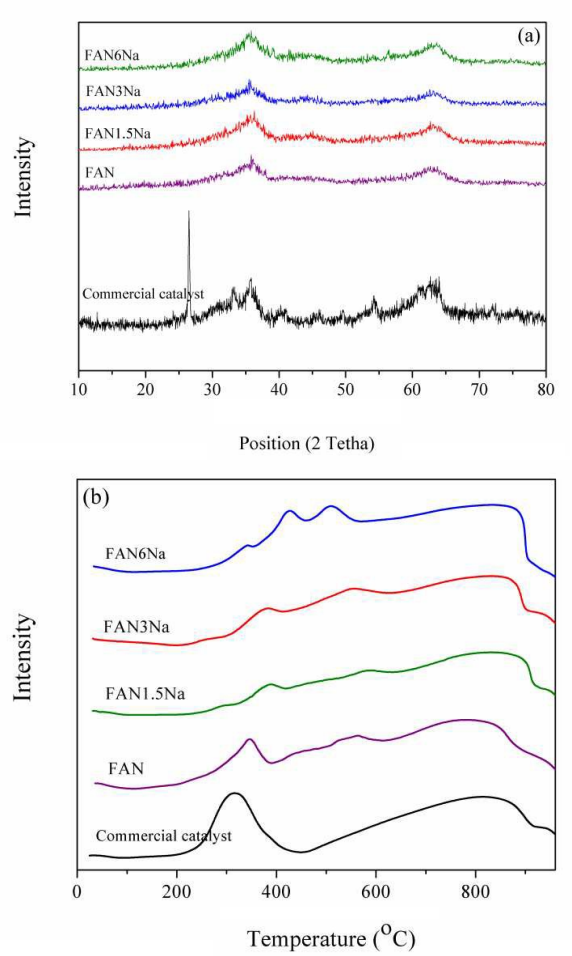

Figure. 6. (a) XRD patterns and (b) TPR profiles of the commercial and FANNa catalysts with different Na contents calcined at 400°C

The catalytic activity of the promoted catalysts with different Na contents are shown in Fig. 7a. It is seen that addition of Na to FAN catalyst improved the CO conversion. The obtained results showed that increasing in Na_2O content up to 3 wt.% increased the CO conversion, but further increase in Na_2O content has a negative effect on the CO conversion. As can be seen, the FAN3Na catalyst exhibited the highest activity among the prepared catalysts at temperatures lower than 450°C. The decrease on the CO conversion of FAN6Na could be related to its lower BET area compared to other promoted catalysts. In addition, the CO conversions of the promoted catalysts were higher than those observed for the commercial catalyst at temperature lower than 450°C.

The long term stability of the FAN3Na catalyst is shown in Figure 7b. As can be seen, this catalyst exhibited stable catalytic performance during 50h time on stream.

The structural properties of the fresh, reduced and spent FAN3Na catalysts are given in Table 2. It is seen that the structural properties of the fresh catalyst significantly changed after the reduction and reaction steps. In the reduction step, the specific surface area and pore volume of the catalyst decreased from 147.7 to 38.8 $m^2\ g^{-1}$ and 0.3 to 0.2 $cm^3\ g^{-1}$, respectively. The results showed that the specific surface area and pore volume of the spent catalyst were lower than the fresh and reduced catalysts. The spent catalyst also exhibited the larger pore and particle sizes compared to the fresh and reduced catalysts.

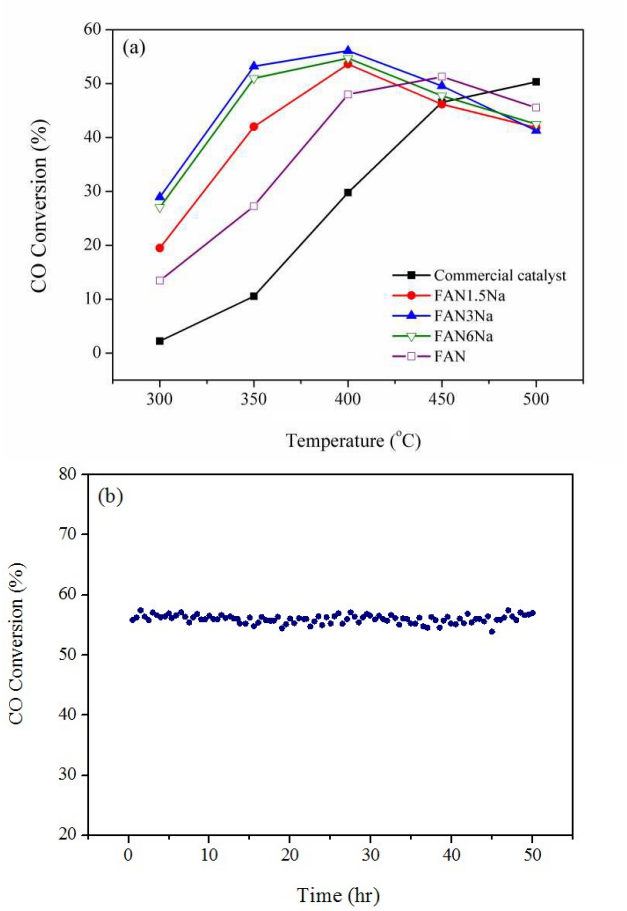

Figure. 7. (a) CO conversion of the commercial and prepared catalysts calcined at 400 °C, (b) long term stability of the FAN3Na catalyst at 400 °C , GHSV= 3×10^4mL/h.$g_{cat.}$ and steam/gas=0.3

The XRD patterns of the fresh, reduced and spent FAN3Na catalysts are presented in Fig. 8a. As can be seen the fresh catalyst showed a low degree of crystallinity, while after the reduction it is well crystallized and all the diffraction peaks in XRD patterns of the reduced and the spent catalysts can be assigned to the magnetite (Fe_3O_4) , an active phase for HTS reaction.

Furthermore, the diffraction peaks of the spent catalyst showed higher intensities compared to those observed for the reduced catalyst, indicating the bigger crystallite size of the spent catalyst.

Fig. 8b shows the pore size distributions and N_2 adsorption/desorption isotherms (upper inset) of the fresh, reduced and spent FAN3Na catalysts. It is seen that in reduction step, the pore size distribution of the catalyst shifted to the larger sizes and the reduced catalyst showed a broad pore size distribution centered at 23 nm. In addition, after 50 h time on stream, the spent catalyst exhibited a very broad pore size distribution indicating a lower surface area compared to the fresh and reduced catalysts.

The N_2 adsorption/desorption isotherms for the fresh, reduced and spent catalysts indicating type IV isotherm with a H2-type hysteresis loop (upper inset) for fresh and reduced catalysts, while after the reaction the type of hysteresis changed and can be classified as type V isotherm with H3-type hysteresis loop. Moreover, for the fresh catalyst the hysteresis loop occurred at low relative pressure confirming a narrow pore size distribution of this sample.

RSC Advances

Cite this: DOI: 10.1039/c0xx00000x

www.rsc.org/xxxxxx

PAPER

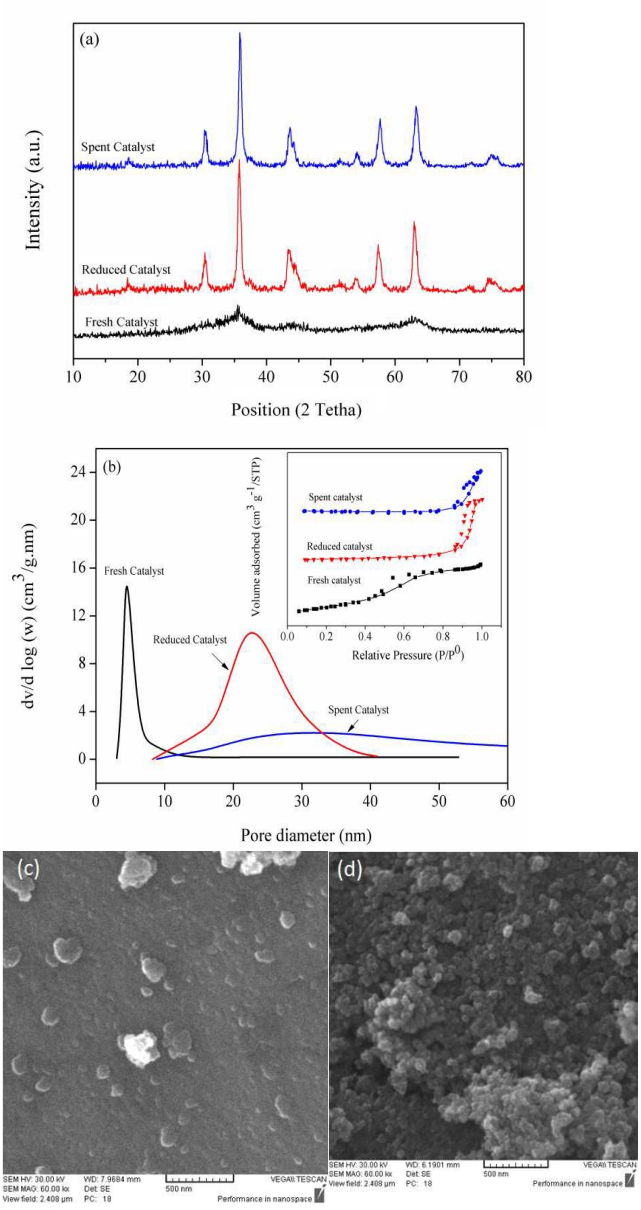

Figure. 8. (a) XRD, (b) Pore size distributions and N_2 adsorption/desorption isotherms of the fresh, reduced and spent FAN3Na catalysts, SEM image of (c) fresh and (d) spent FAN3Na catalyst after 50 h time on stream

For the reduced and spent catalysts the hysteresis loop was observed at higher relative pressure indicating broader pore size distribution of these samples.

The SEM images of the fresh and spent FAN3Na catalysts are shown in Fig. 8c and 8d, respectively. It is seen that the particles in spent catalyst were agglomerated together and this catalyst exhibited bigger particle size compared to that observed for the fresh catalyst.

The TEM images of the fresh and spent FAN3Na catalysts are also presented in Fig.9 , respectively. As can be seen in spent catalyst the crystals are bigger than those observed in fresh catalyst. The increase in crystal size could be related to sintering of iron crystals under the reaction conditions, which is accompanied by a loss in the BET surface area and an increase in particle size as shown in Table 2.

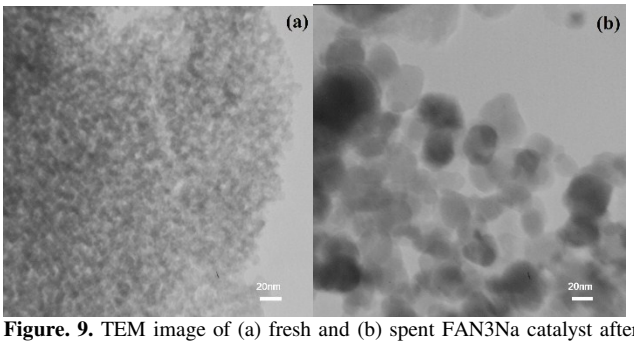

Figure. 9. TEM image of (a) fresh and (b) spent FAN3Na catalyst after 50 h time on stream

Conclusion

In this work the effect of alkali promoters (Na, K, Cs and Li) on the CO removal performance of Cr-free Fe-Al-Ni catalysts in high temperature water gas shift reaction is investigated. BET analysis showed that the prepared catalysts possessed high surface area and mesoporous structure. In the XRD patterns of all prepared catalysts only hematite phase was detected and no separate crystalline phases ralated to the Al, Ni or other promoters were observed. In addition, from the TPR analysis, it was found that addition of Li to the Fe-Al-Ni catalyst shifted the reduction temperature of $Fe_2O_3 \rightarrow Fe_3O_4$ to lower values while addition of Na and K to the Fe-Al-Ni catalyst increased the reduction temperature of hematite to magnetite phase. It can be concluded from the HTS activity test that by addition of alkali promoters to the FAN catalysts, the CO conversion improved and the methanation reaction suppressed. The results revealed that Na promoter exhibited the highest positive effect on CO conversion and suppression of methanation. The results of TPD analysis confirmed that addition of Na to the FAN catalyst (FANNa) increased the intensity of the CO and CO_2 desorption peaks indicating more basic sites over this catalyst, which is the reason of higher catalytic performance and methane suppression of this catalyst compared to unpromoted FAN catalyst. In particular, 3wt.% Na promoted Fe-Al-Ni catalyst exhibited higher CO conversion than the commercial Cr-containing catalyst and showed high stability during 50h time on stream under the reaction.

The remarkable catalytic performance of FANNa catalyst is mainly ascribed to the synergy effect of Al as a textural promoter by increasing BET surface area and thermal stability of iron oxide. Based on the obtained results the Fe_2O_3-Al_2O_3-NiO-Na_2O catalyst can be considered as a promising chromium-free catalyst for high temperature water gas shift reaction.

Acknowledgements

The authors are grateful to National Petrochemical Company, Research and Technology Company (NPC-RT) for supporting this work.

References

1. P. Carson P, C. Mumford, Hazardous chemicals handbook. 2nd ed. Great Britain: Butterworth-Heinemann; 2002. p. 148-51.
2. Committee for medicinal products for human use (CHMP). Guideline on the specification limits for residues of metal catalysts or metal reagents (Doc. No. EMEA/CHMP/SWP/4446/ 2000). London, U.K: European Medicines Agency; February 2008.
3. M. Marafi, A. Stanislaus, E. Furimsky, Handbook of spent hydroprocessing catalysts. Amsteram and Oxford: Elsevier; 2010. p. 93-120.
4. J.Y. Lee , D-W. Lee, Y-K. Hong, K-Y. Lee, *Int. J. Hydrogen Energy* . 2011, **36**, 8173-8180
5. F.A. de Bruijn, B. Rietveld, R.W. van den Brink, Catalysis for Renewables, in: G. Centi, A. van Santen (Eds.), Wiley-VCH, Weinheim, 2007, pp. 299–336.
6. K. Babita, S. Sridhar, K.V. Raghavan, *Int. J. Hydrogen Energy,* 2011*,* **36,** 6671–6688.
7. J.Y. Lee, D-W. Lee, M.S. Lee, K-Y. Lee, *Catal Commun,* 2011, **15**, 37–40
8. F. Bustamante, R.M. Enick, R.P. Killmeyer, B.H. Howard, K.S. Rothenberger, *Am. Inst. Chem. Eng. J.* 2005*,* **51**, 1440–1454.
9. E.B. Quadro, M. de Lourdes, R. Dias, A.M.M. Amorim, M. do Carmo Rangel, *J. Braz. Chem. Soc*. 1999, **10,** 51–59.
10. A. Haryanto, S.D Fernando, S.D. Filip To, P.H. Steele, L. Pordesimo, S. Adhikari, *J. Thermodyn. Catal.* 2011*,* **2**, 1000106
11. F. Meshkani, M. Rezaei, *J. Ind. Eng. Chem.* 2014, **20,** 3297–3302
12. A. Andreev, V. Idakiev, D. Mihajlova, D. Shopov, *Appl. Catal.* 1986, **22,** 385-387.
13. K. Kochloefl, in: G. Ertl, H. Kno¨ zinger, J. Weitkamp (Eds.), Handbook of Heterogeneous Catalysis, vol. 4, Wiley-VCH, Weinheim, 1997, pp. 1831–1843.
14. Official Journal of the European Union, 2003, **46**, 19–37.
15. F.M. Gottschalk, R.G. Copperthwaite, M.V.D. Riet, G.J. Hutchings, *Appl. Catal*. 1988, **38,** 103–108.
16. G.C. Arau´ jo, M.C. Rangel, *Catal. Today*, 2000, **62**, 201–207.
17. S. Natesakhawat, X. Wang, L. Zhang, U.S. Ozkan, *J. Mol. Catal. A.* 2006*,* **260**, 82–94.
18. F.M. Gottschalk, G.J. Hutchings, *Appl. Catal*. 1989, **51**, 127–139.
19. L. Zhang, J.M.M. Millet, U.S. Ozkan, *Appl. Catal. A*. 2009, **357**, 66–72
20. Y.S. Oh, H.S. Roh, K.W. Jun, Y.S. Baek. *Int. J. Hydrogen. Energy.* 2008**, 28,** 1387-92.
21. D. Harshini, Y. Kwon, J. Han, S.P. Yoon, S.W. Nam, T.H. Lim. *Korean J Chem. Eng*. 2010, **27,** 480-6.
22. S.H.Park, B.H. Chun, S.H. Kim, *Korean. J. Chem.Eng*. 2001**, 28**, 402-8.
23. S.H. Kim, S.W. Nam, T.H. Lim, H.I. Lee*, Appl. Catal. B. Environ.* 2008*,* **81**, 97-104.
24. K. Watanabe, T. Miyao, K. Higashiyama, H. Yamashita, M. Watanabe, Catal Commun 10 (2009) 1952-5.
25. L. Huang, J. Xie, R. Chen, D. Chu, W. Chu, A.T. Hsu, *Int. J. Hydrogen Energy.* 2008, **33**, 7448-56.
26. M. Feyzi, A.A. Mirzael, H.R. Bozorgzadeh*, J. Nat. Gas. Chem.* 2010*,* **19,** 341-53.
27. K-R. Hwang, C.-B. Lee, J.-S. Park, *J. Power Sources*. 2011, **196,** 1349.
28. F. Meshkani, M. Rezaei, *Renewanle energy*, 2015,**74**, 588-598
29. K.S.W. Sing, D.H. Everett, R.A.W. Haul, L. Moscou, R.A. Pierotti, J. Rouque´ rol, T. Siemieniewska, *Pure. Appl. Chem*. 1985, **57,** 603.
30. M. Kruk, M. Jaroniec, *Chem. Mater*. 2001, **13,** 3169.
31. L. Zhang, X. Wang, J-M.M. Millet, P.H. Matter , U.S. Ozkan, *Applied Catalysis A: General*, 2008, **351,** 1–8
32. M.E. Dry, L.C. Ferreira, *J. Catal*.1967**, 7**, 352.
33. P.S. Sidhu, R.J. Gilkes, M. Posner, *J. Inorg. Nucl. Chem.* 1978, **40** 429.
34. Z. Gao, Y. Feng, F. Cui, Z. Hua, J. Zhou, Y. Zhu, J. Shi, *J. Mol. Catal. A: Chem.* 2011, **336**, 51–57.
35. X. Wang, G. Li, U.S. Ozkan, *J. Mol. Catal. A*. 2004, **217**, 219.
36. M.E. Dry, G.J. Oosthuizen, J. Catal. 11 (1968) 18.
37. J.W. Niemantsverdriet, A.M. vander Kraan, W.L. van Dijk, H.S. vander Baan, *J. Phys. Chem.* 1980, **84,** 3363.
38. H. K¨olbel, Kalium als strucktureller und Energetischer Promotor in Eisenkatalysatoren, in: Actes du Deuxieme Congress International de Catalyse, vol. II, Tchnip, Paris, 1960, p. 2075.
39. D.G. Miller, M. Moskovits, *J. Phys. Chem.* 1988, **92**, 6081.
40. H. Wan, B. Wu, C. Zhang, H. Xiang, Y. Li, , *J. Mol. Catal. A, 2008,* **283**, 33–42
41. K.R. Hwang, C.B. Lee, J.S. Park, *J. Power. Sources* 2011*,* **196,** 1349–1352.
42. S.H. Kim, J.H. Chung, Y.T. Kim, J. Han, S.P. Yoon, S.W. Nam, H.I. Lee, *Int. J. Hydrogen Energy*. 2011, **35** 3136–3140.